Nonlinear mechanical and poromechanical analyses : comparison with analytical solutions

Mountaka Souley, Alain Thoraval

Nonlinear mechanical and poromechanical analyses: comparison with analytical solutions

M. Souley* and A. Thoraval
INERIS, Ecole des Mines de Nancy, FRANCE
*Corresponding author: Ecole des Mines, Parc de Saurupt, CS 14234 F-54042 Nancy cedex,
Mountaka.Souley@ineris.fr

Abstract: The validation of computational schemes for modeling multiphysic phenomena in porous geomaterials is a key importance in geoenvironmental applications. This paper focuses on the validation of nonlinear and coupled hydromechanical schemes by comparing the results of numerical predictions performed with COMSOL and the mathematical solutions. Firstly, we simulate the nonlinear mechanical behavior of rock mass around a deep cylindrical hole. The second example treats on the simulation of the well-known one-dimensional consolidation of a saturated porous rock column. Finally a validation of poroelastic calculations related to a cylindrical hole excavation in a saturated porous media is achieved.

Keywords: Nonlinear behavior, elastoplasticity, hydromechanical coupling, code verification, analytical solutions.

1. Introduction

Waste storage problems, as well as the natural resource management (water, gas or hydrocarbons), explain the increased interest of the scientific community to study the multiphysic behavior of rock masses. Typically, the long-term behavior of the underground excavations is a social and economic challenge particularly in the contexts of post-mining or radioactive waste storage. Despite the constraints imposed by geological considerations, attention has been directed by developing mathematical and numerical models of the thermo-hydro-mechanical behavior of saturated geological media (Tsang 1987, Tsang 1991, Bear et al. 1993, Selvadurai and Nguyen 1995, Jing et al. 1995, Stephanson et al. 1996, Rutquist et al. 2001). Those numerical modelings are currently used to understand and forecast the complex behavior of the rock mass around the underground cavities. In order to accurately perform these multiphysic modelings at large space and time scales, it is necessary to check the capacity of these codes, to precisely reproduce the correct response in the case of some problems for which analytical solutions exist in the field of geomechanics. This is an important step before evaluating the ability of the code to correctly reproduce laboratory or in situ measurements or specific experiments.

This paper focuses on comparing the results of numerical predictions with mathematical solutions. The code COMSOL is used in the framework of nonlinear mechanics and hydromechanical couplings of saturated porous media through three verification cases.

The first is focused on the nonlinear mechanical behavior. The second concerns the hydromechanical modeling of the one-dimensional consolidation, where a column of fluid-saturated porous medium of finite length is subjected to a surface load. The third case involves the excavation of a deep cylindrical hole in a saturated porous rock and subjected to an anisotropic stress field.

2. Theoretical background and COMSOL implementation

The classical dealing on the process of consolidation in one-dimension inducing isothermal fluid flow through a deformable porous medium was firstly addressed by Terzaghi (1925) and later developed and generalized by Biot (1941) in three dimensions. The theory assumes linear elasticitity to characterize the mechanical behavior of the porous solid and Darc's law for fluid flow through the porous medium. Within the framework of an extension to poroplasticity, Coussy (1995) has shown the existence of a plastic effective stress when the volumetric plastic strain (ε_v^p) and plastic porosity (θ^p) are related by a linear form. This plastic effective stress is, in general case, different to the elastic ones and results in defining a plastic Biot coefficient (scalar or tensor).

The constitutive equations (equilibrium equation, mechanical constitutive behavior, law of effective stresses according to Biot's concept and fluid diffusivity equation which combines Darcy's law and fluid mass conservation) are expressed in a general way as follows:

$$\begin{cases} -\nabla \underline{\underline{\sigma}} = \rho_{und}\boldsymbol{g} = \rho_f \phi + \rho_d \boldsymbol{g} \\ \underline{\underline{\sigma'}} - \underline{\underline{\sigma_0}}' = \underline{\underline{\underline{\underline{C_0}}}} : \underline{\underline{\varepsilon}} - \underline{\underline{\varepsilon^p}} \\ \underline{\underline{\sigma'}} - \underline{\underline{\sigma_0}}' = \underline{\underline{\sigma}} - \underline{\underline{\sigma_0}} + b\ p - p_0\ \underline{\underline{I}} \\ \rho_f S \frac{\partial p}{\partial t} + \nabla . \rho_f \left[-\frac{k_{int}}{\mu_f} \nabla p + \rho_f \boldsymbol{g} \right] = -\rho_f b \frac{\partial\ tr\underline{\underline{\varepsilon}}}{\partial t} + Q_m \end{cases} \quad [1]$$

where $\underline{\underline{\sigma}}$, $\underline{\underline{\sigma'}}$ ($\underline{\underline{\sigma_0}}$, $\underline{\underline{\sigma_0}}'$) are total and effective (initial) stress tensor [Pa]; p (p_0) is the (initial) fluid pore pressure [Pa]; b is the Biot coefficient [-]; ρ_{und} and ρ_d represent undrained and drained densities of porous medium [kg/m^3]; ρ_f is fluid density [kg/m^3]; $\underline{\underline{\underline{\underline{C_0}}}}$ is the tensor of drained elastic modules [Pa]; $\underline{\underline{\varepsilon}}$ is total strain tensor; $\underline{\underline{\varepsilon^p}}$ is the irreversible (plastic) strain of squeleton [-]; k_{int} is the intrinsic permeability of the porous medium [m^2]; **g** denotes the gravity vector [m/s^2]; μ_f is the fluid dynamic viscosity [Pa.s]; S is the storage coefficient (representing the inverse of the Biot modulus here) [1/Pa]; Q_m is the additional source term [kg/m^3/s].

Plasticity is the first nonlinearity of the mechanical behavior of geomaterials and appears primarily in the instantaneous response, but also in the long term as a consequence of strength reduction with time. In general, a plastic model is characterized by:

- a yield function (or criterion), $F\ \underline{\underline{\sigma}}$;
- a hardening/softening function and flow rule, $G\ \underline{\underline{\sigma}}$.

The yield function defines the stress combination for which plastic flow takes place. These functions are represented by one or more limiting surfaces in a generalized stress space with points below or on the surface being characterized by an incremental elastic or plastic behavior, respectively. The flow rule specifies the direction of the plastic strain increment vector as that normal to the potential surface: it is called associated if the potential and yield functions coincide $F = G$, and non-associated otherwise.

The implementation of elastoplastic material in COMSOL is based on the additive decomposition of total strain (assumption of small strains). Thus, the stress-strain relationship is given by the second equation of system (1). The plastic strain tensor $\underline{\underline{\varepsilon^p}}$ and a vector κ of state parameters describe the state of the plastic strain. The evolution of these variables is governed by the following rate equations:

$$\dot{\underline{\underline{\varepsilon}}}^p = \lambda \frac{\partial G\ \underline{\underline{\sigma}},\ \underline{\underline{\varepsilon^p}},\ \kappa}{\partial \underline{\underline{\sigma}}} \quad \text{and} \quad \dot{\kappa} = -\lambda \frac{\partial G\ \underline{\underline{\sigma}},\ \underline{\underline{\varepsilon^p}},\ \kappa}{\partial \kappa} \quad [2]$$

where λ is the plastic multiplier determined by the complementary conditions (also called consistency rule):

$$F\ \underline{\underline{\sigma}},\ \underline{\underline{\varepsilon^p}},\ \kappa \le 0 \quad \lambda \ge 0 \quad F\ \underline{\underline{\sigma}},\ \underline{\underline{\varepsilon^p}},\ \kappa\ \lambda = 0$$
$$or \quad [3]$$
$$\begin{cases} F\ \underline{\underline{\sigma}},\ \underline{\underline{\varepsilon^p}},\ \kappa < 0 & \lambda = 0 \\ F\ \underline{\underline{\sigma}},\ \underline{\underline{\varepsilon^p}},\ \kappa = 0 \quad dF\ \underline{\underline{\sigma}},\ \underline{\underline{\varepsilon^p}},\ \kappa = 0 & \lambda > 0 \end{cases}$$

Mohr-Coulomb or Hoek and Brown criterions generally used in geomechanics present the disadvantage of being expressed according to the extreme stresses (minor and major: σ_3, σ_1). This leads to difficulties related to their numerical implementation in the case of complex stress paths (particularly in the vicinity of corners).

To avoid that, it is better to use criteria which utilize the three principal stresses. For instance, the Drucker-Prager shear criterion is represented in the principal stress space (σ_1, σ_2, σ_3) by a cone with axis along the octahedric line ($\sigma_1 = \sigma_2 = \sigma_3$). The Mohr-Coulomb shear criterion, characterized by the cohesion, C, and friction angle, φ, is represented by an irregular hexagonal pyramid. The parameters q_φ and k_φ (intervening in the Drucker-Prager criterion) can be adjusted so that the Drucker-Prager cone will either pass through the outer or the inner edges of the Mohr-Coulomb pyramid.

For instance, the inner adjustment allows expressing the Drucker-Prager yield function as follows:

$$F\ \underline{\underline{\sigma}} = F\ \ p,q\ = q + q_\varphi \sigma_m - k_\varphi = q + \frac{6\ sin\varphi}{3 + sin\varphi}\sigma_m - \frac{6\ C\ cos\varphi}{3 + sin\varphi} \quad [4]$$

where q is the deviatoric (von Mises) stress; σ_m is the mean stress $tr\underline{\underline{\sigma}}/3$.

Finally, for seek of simplicity we consider a standard material (G = F). Also, in order to compare to analytical solution, we assume an elastic perfectly plastic behavior.

3. Nonlinear mechanical validation

Firstly, the problem concerns the determination of stresses and displacements distribution around a cylindrical hole in an

infinite elastoplastic medium subjected to initial stresses. The medium is assumed to be linearly elastic, perfectly plastic, with a failure surface defined by the Drucker-Prager criterion (Eq. 4) with the associated flow rules leading to a maximum of material dilatancy.

An isotropic in situ stress state, σ_0, exists with stresses equal to -13.7 MPa (compressive stresses are negative). It is assumed that the problem is symmetric with respect to both the horizontal and vertical axes. The hole radius , r_0, is 3 m and is assumed to be small compared to the length of the cylinder. This permits the use of the plane-strain condition, even if the problem is, in this case, 1D and then could be solved with axisymmetric configuration. The geometrical model and boundary conditions used in COMSOL are shown on figure 9 without the hydraulic ones. The input parameters are : E_0 (Young modulus) = 5800 MPa; ν_0 (Poisson ratio) = 0.3; C = 1 MPa and φ = 25°.

When the failure surface is defined by the Mohr-Coulomb criterion, the analytical solution for this problem is provided in terms of stresses and displacements by Salencon (1969) for both associated plastic flow and non-associated plastic flow. The yield zone radius (or plastic radius), r_p, is given analytically by:

$$r_p = r_0 \left(\frac{2}{K_p + 1} \frac{\sigma_0 + \frac{C_q}{K_p - 1}}{pi + \frac{C_q}{K_p - 1}} \right)^{\frac{1}{K_p - 1}} \qquad [5]$$

where p_i is the internal pressure at the hole wall (considered as null here);

$C_q = 2\, C \tan\left(\frac{\pi}{4} + \frac{\varphi}{2}\right)$ and $K_p = \frac{1 + sin\varphi}{1 - sin\varphi}$.

The author also proposes the distribution of radial and orthoradial stresses as well as radial displacement in the two domains: plastic ($r \leq r_p$) and elastic ($r > r_p$), where r is the distance from the hole center. For more details, the reader could consult Salençon (1969).

Figures 1 and 2 show a direct comparison between *COMSOL* results and the analytical solution along a radial line. The small differences between the numerical and analytical results is essentially related to numerical scheme: (a) use of the inner cone to adjust the Mohr-Coulomb pyramid, and (b) use of the three principal stresses rather than the two extreme stresses.

In a second step, we consider now an anisotropic stress state of: σ_{x0} = -16.1 MPa; σ_{y0} = -12.7 MPa; σ_{a0} = -12.4 MPa, leading to an averaged mean stress of -13.7 MPa.

In this case, there is no analytical solution in the literature. We will thus compare the numerical results with the previous analytical solution by assuming an isotropic stress equal to a mean stress of -13.7 MPa.

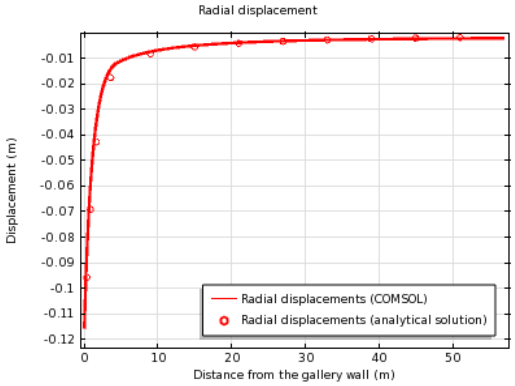

Figure 1. Radial displacement along a radial line.

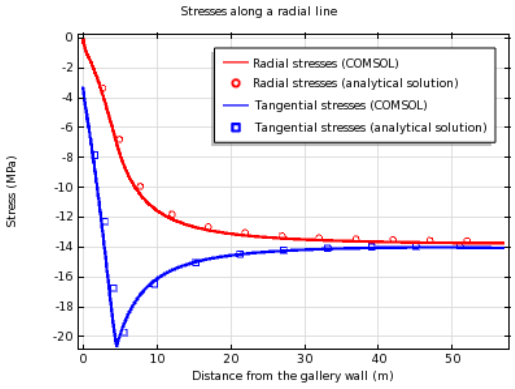

Figure 2. Radial and tangential stresses along a radial line.

Figure 3 represents the contours of the von Mises deviatoric stress. In relation to the development of plastic zone (resulting from stress corrections) the maximum deviatoric stress is reached at the interface between elastic and plastic domains.

Figure 4 shows a direct comparison between *COMSOL* results (in terms of radial displacement along horizontal and vertical lines) and the analytical solution assuming an isotropic initial stress state of -13.7 MPa. It is interesting to note that the radial displacement obtained from the analytical solution is the average of the predicted radial displacements in the horizontal and vertical directions.

Figure 5 illustrates the variation of tangential and radial stresses. The evolution of

the predicted curves is qualitatively in adequacy with that we already analytically discuss.

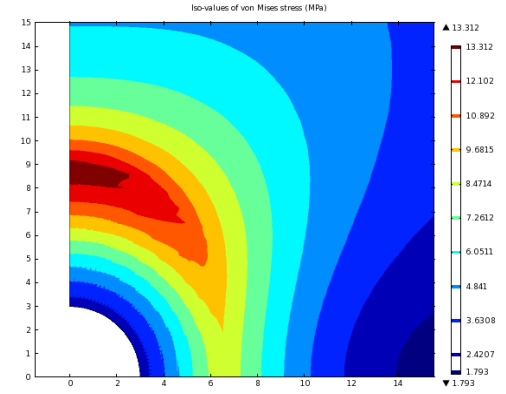

Figure 3. Contours of von Mises stress : anisotropic initial stresses.

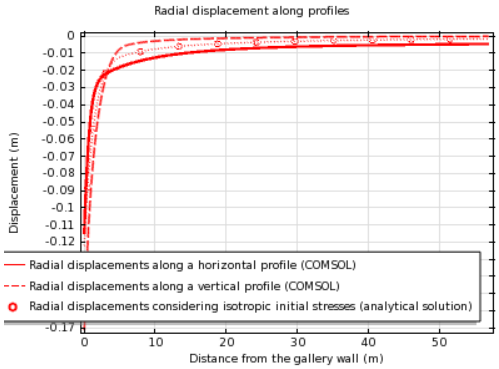

Figure 4. Radial displacement along horizontal (θ=0°) and vertical (θ=90°) lines compared to mean analytical solution : anisotropic initial stresses.

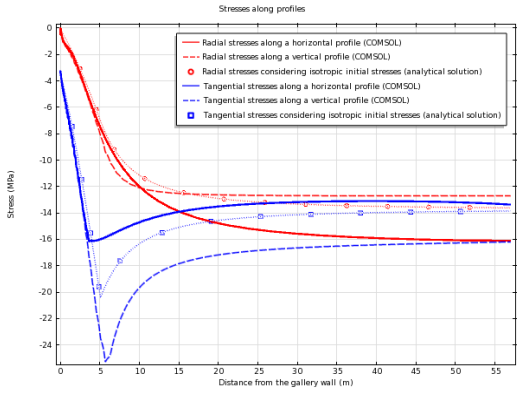

Figure 5. Tangential and radial stresses along horizontal (θ=0°) and vertical (θ=90°) lines compared to mean analytical solution: anisotropic initial stresses.

These figures clearly indicate the coherence of the numerical results computed in the framework of nonlinear mechanics of geomaterrials.

4. Poromechanical validation

4.1 One dimensional consolidation

We consider the problem of a one-dimensional column of 20 m height of a saturated poroelastic medium. Initially, stresses and pressure are assumed to be equal to zero. No displacements are assumed on boundaries except on the top limit where a constant surface load, $\sigma_{z0} = 10^5$ Pa, is applied. During phase 1, no flux boundaries are applied (undrained condition). During phase 2, the impervious boundary condition at the top is replaced by a zero pressure condition (drained condition).

The soil matrix is homogeneous and behaves elastically; the isotropic Darcy's transport law is assumed. The applied pressure is initially carried by the fluid (during phase 1) but, as time goes on (during phase 2), the fluid drains through the top of layer surface, transferring the load to the soil matrix. The solution to this one-dimensional consolidation problem is derived in the framework of Biot theory by solving Eq. 1. (Detournay and Cheng, 1993).

The pore pressure value, p_0, reached at the end of phase 1, can be derived from the fluid constitutive law considering undrained conditions and using the one-dimensional mechanical constitutive law, say finally the Skempton's equation:

$$p_0 = -\frac{bM\sigma_{z0}}{K_0 + 4G/3 + b^2M} \qquad [6]$$

where K_0 is the drained bulk modulus; G is the shear modulus; M is the Biot's modulus.

The closed-form solution from Detournay and Cheng (1993) is expressed in terms of vertical displacement (or subsidence) u_z and pore pressure as follows:

$$\hat{u}_z = -2b\frac{p_0}{\sigma_0}\left(\sum_{k=0}^{\infty}\frac{\cos\ a_k\hat{z}}{a_k^{\ 2}}\exp\ -a_k^{\ 2}\hat{t}\right) + \hat{z} - 1$$
$$p = 2p_0\sum_{k=0}^{\infty}\frac{\sin\ a_k\hat{z}}{a_k}\exp\ -a_k^{\ 2}\hat{t} \qquad [7]$$

where $\hat{u}_z = -\frac{K_0 + 4G/3}{\sigma_0}\frac{u_z}{L}$, $a_k = \frac{\pi}{2}\ 2k+1$, $\hat{t} = \frac{\chi t}{L^2}$,

$\hat{z} = \frac{L-z}{L}$, χ is the fluid diffusivité [m^2/s].

For the numerical application, we consider a layer of soil of large lateral extent, and thickness L = 20 m. The drained Young modulus E_0 is 3435 MPa, and the Poisson coefficient ν_0 is 0.12. The density of the dry rock ρ is 2750 kg/m^3, the density of water ρ_f is 1000 kg/m^3, the water bulk modulus K_f is 2000 MPa, the intrinsic permeability k_{int} is 5 10^{-20} m^2. The Biot modulus, M, and coefficient, b, are 5112 MPa and 0.6, respectively. Also, gravity is set to 9.81 m/s^2.

The contours of subsidence (vertical displacement) at selected fluid-flow time corresponding to 10^{10} s (or ~317 years) are plotted in figure 6. A maximum of 0.56 mm is reached at the top.

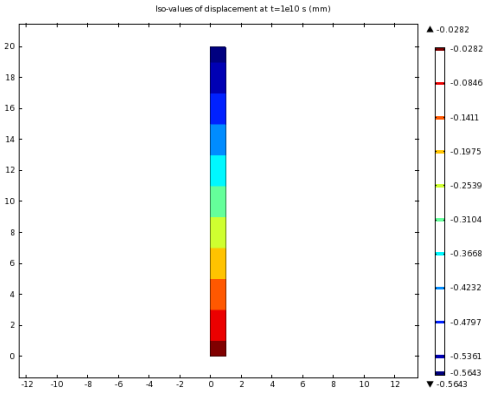

Figure 6. Contours of cummulative subsidence at the end of phase 2 (at t = 10^{10} s).

The numerical solution for pore pressure and vertical displacement, along the column are evaluated and compared to the analytical solution at four different times (10^7, 10^8, 10^9 and 10^{10} s). The results are plotted versus the distance, d, from the top of surface (corresponding to d = 0).

The simulation results are in very good agreement with the analytical solution for pore water pressure dissipation (figure 7), time-dependent surface displacement (figure 8), and also stresses (not presented herein).

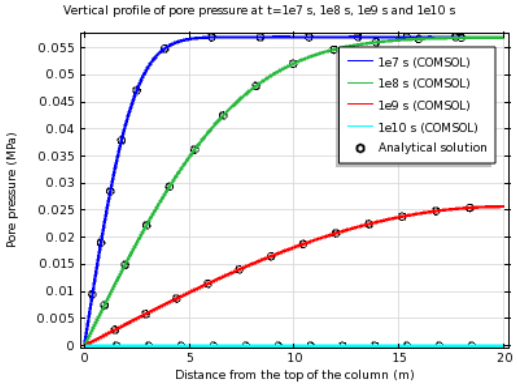

Figure 7. Profile of pore pressure as a function of distance from the top surface for flow time ranged between 10^7 and 10^{10} s.

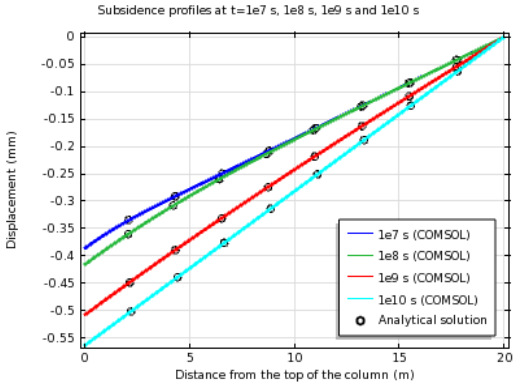

Figure 8. Profile of subsidence as a function of distance from the top surface for flow time ranged between 10^7 and 10^{10} s.

4.2 Poroelastic response of a borehole

A borehole is excavated in a saturated porous rock subject to an anisotropic in situ stress field. The borehole boundary is free to drain and is exposed to atmospheric pressure. The initial pore pressure field is p_0. The problem is analyzed assuming plane-strain conditions and instantaneous drilling of the borehole. The numerical simulation allowed to capture the poroelastic effects taking place during the short time response of the system. The initial and boundary conditions (mechanic and hydraulic) are summarized in figure 9. The hydromechanical parameters are the same than in the previous section.

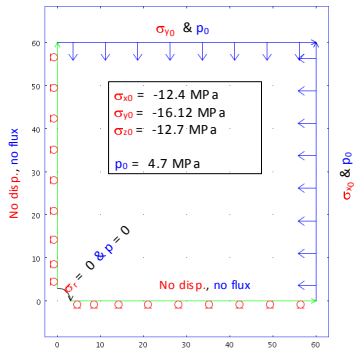

Figure 9. COMSOL model : geometry and boundary conditions of 2D consolidation.

The two-dimensional poroelastic solution for a borehole in an anisotropic stress field can be found in Detournay and Cheng (1988). The general solution is derived in the Laplace transform domain and results in the time domain can be obtained using a numerical inversion technique. The solution is formulated by superposition of asymptotic solutions for three loading modes: (1) a far-field isotropic stress: this loading mode produces the classical Lamé solution in elasticity (known also as Kirsh solution); (2) an initial pore pressure distribution that induces short-time asymptotic solution for stresses, pore pressure and displacements; and (3) a far-field stress deviator. The radial, tangential and shear stresses (σ_r , σ_θ , $\sigma_{r\theta}$) in polar coordinates, pore pressure (p), and radial and tangential displacements (u_r , u_θ) induced by each loading mode are formulated. The equations relating to the fundamental solutions of these 3 load patterns can be consulted in Detournay and Cheng (1988).

Due to the instantaneous undrained response in an anisotropic initial stress field, over-pressures develop in the direction of the initial minor stress, and under-pressures in the direction of the initial major stress, in accordance with the analytical solution. Indeed in relation to the anisotropy of the initial stress state, the instantaneous response induced a variation (increase and reduction, respectively in the horizontal and vertical directions) of the mean stress, which in return by Skempton effect, involves a variation (positive and negative) of the pore pressure. It is not the case when the initial stress state is isotropic. Figure 10 presents the contours of pore pressure after $t = 10^6$ s of drainage. Even at this time, one can notice the presence of these over-pressures (not yet dissipated) in the horizontal direction and under-pressures in the vertical direction inside the solid mass. Finally, the contours of total displacement resulting to the coupled hydro-mechanical effects are illustrated in figure 11 at $t = 10^6$ s.

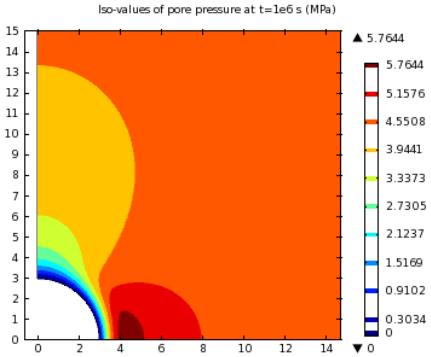

Figure 10. COMSOL model : contours of pore pressure for 2D consolidation ($t=10^6$ s).

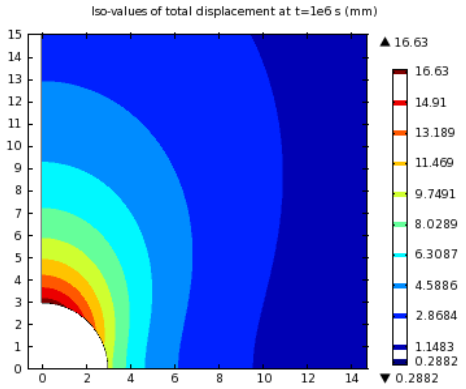

Figure 11. COMSOL model : contours of total displacement for 2D consolidation ($t=10^6$ s).

Isochrones of pore pressure variation with distance from the hole wall are compared to the analytical solution in figure 12 for $t = 10^6$ s, and the direction $\theta = 0$ and 90° (with respect to the x-axis). The steep radial gradient of pore pressure developing at the borehole wall is illustrated in this figure. This gradient is associated with a rapid drainage of fluid near the borehole which influences the apparent stiffness properties of the rock.

The radial displacement versus the distance from the hole wall at $\theta = 0$ and 90° is compared to the analytical solution in figure 13 for a simulation time of 10^6 s. Figure 14 summarizes the profiles of radial and orthoradial stresses between numerical and analytical solution.

From these figures, we can notice that the results of the *COMSOL* simulations show a

very good agreement with the analytical predictions.

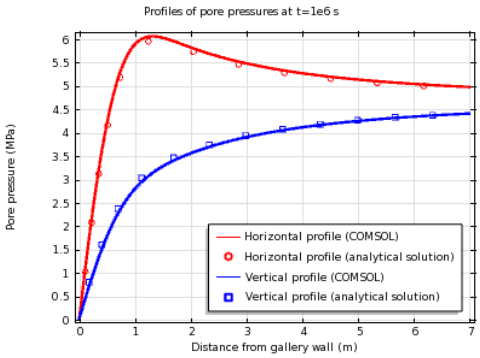

Figure 12. Pore pressure variation with the distance from the hole wall at θ = 0° and 90° (t = 10^6 s).

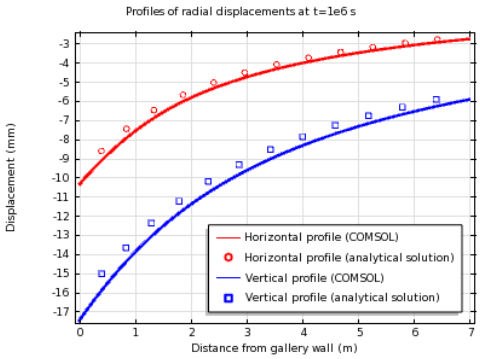

Figure 13. Radial displacement variation with the distance from the hole wall at θ = 0° and 90° (t = 106 s).

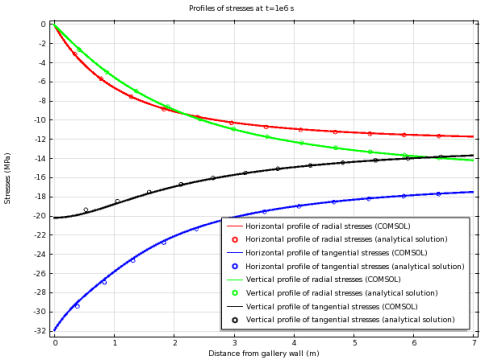

Figure 14. Radial and tangential stresses variation with the distance from the hole wall at θ = 0° and 90° (t = 10^6 s).

5. Concluding remarks

Numerical modeling are currently used to understand and forecast the complex rock mass behavior around the underground structures where several physics and their couplings are present. In order to accurately perform these multiphysic modelings at large scales, it is necessary to check the capacity of these codes, to correctly reproduce the phenomena through some simple stress load paths. This paper presents this exercise of validation where numerical simulations were performed with COMSOL

First, we simulate the nonlinear mechanical behavior (elastoplasticity) of rock mass around a deep cylindrical hole and successfully compare with the analytical solution (Salençon 1969).

The second example treats on the simulation of one-dimensional consolidation of a column of saturated porous rock in the framework of poroelasticity. The simulation results are in very good agreement with the analytical solution (Detournay and Cheng, 1993) in terms of pore pressure dissipation, time-dependent subsidence and stresses.

Thirdly, a borehole is excavated in a saturated porous rock subject to an anisotropic in situ stress field. Here also, the fields of displacement, pore pressure and stresses numerically predicted are successfully compared with those obtained by the semi-analytical solution proposed Detournay and Cheng (1988).

Next stage of this work concerns in particular the following applications: (a) study of water effects on the stability of slopes and underground cavities, (b) dimensioning of CO_2 storage sites. These applications require complementary developments (such as poroplasticity of saturated and unsaturared porous media) which will have to also be validated.

6. References

1. Bear J., C.-F.Tsang and G. de Marsily (Eds) Flow and Contaminant transport in Fractured Rock, Academic Press, New York, (1993)

2. Biot M.A., General theory of three-dimensional consolidation, J Appl Phys, **12**, 155–64, (1941)

3. Coussy O., Mechanics of porous continua, Wiley Ed, (1995)

4. Detournay E. and A. H.-D. Cheng, Poroelastic Response of a Borehole in a Non-Hydrostatic Stress Field, Int. J. Rock Mech. Min. Sci. & Geomech. Abstr., **25(3)**, 171-182 (1988)

5. Detournay E. and A. H-D. Cheng, Fundamentals of Poroelasticity, in Comprehensive Rock Engineering, J. Hudson, E. Hoek, E. T. Brown and C. Fairhurst, Eds. London: Pergamon Press, **2**, 13-171. (1993)
6. Jing L., C.-F.Tsang and O. Stephansson, DEOCOVALEX – An international co-operative research project on mathematical models of coupled THM processes for safety analysis of radioactive waste repositories, Int. J. Rock Mech. Min. Sci. Geomech. Abstr. **32(5)**, 389–398 (1995)
7. Rutqvist J., Borgesson J, Chijimatsu M, Kobayashi A, Jing L, Nguyen TS, Noorishad J, and C-F. Tsang, Thermohydromechanics of partially saturated geological media: governing equations and formulation of four finite element models, Int J Rock Mech Min Sci, **38(1),** 105**–**28, (2001)
8. Salencon J., Contraction Quasi-Statique D'une Cavité a Symétrie Sphérique Ou Cylindrique Dans Un Milieu Elastoplastique, Annales Des Ponts Et Chaussées, **4**, 231-236 (1969)
9. Selvadurai A.P.S. and T.S. Nguyen, Computational modelling of isothermal consolidation of fractured media, Computers and Geotechnics, 17, 39-73, (1995)
10. Stephansson O., L. Jing and C.-F. Tsang, Mathematical and Experimental Studies, Developments in Geotechnical Engineering, (Eds) Coupled Thermo-Hydro-Mechanical Properties of Fractured Media, 79, Elsevier, Amsterdam, (1996)
11. Tsang C.-F., (Ed) Coupled Processes Associeated with Nuclear Waste Repositories, Academic Press, New York, (1987)
12. Tsang C-F., Coupled thermo-mechanical hydro-chemical processes in rock fractures. Rev Geophys, **29**, 537–51, (1991)